Prediction of the Propagation of Trajectory Uncertainty for Climbing Aircraft

Thomas Zeh
Chair for Air Transport Technology and Logistics
Technische Universität Dresden
Dresden, Germany
thomas.zeh@tu-dresden.de

Judith Rosenow
Chair for Air Transport Technology and Logistics
Technische Universität Dresden
Dresden, Germany
judith.rosenow@tu-dresden.de

Richard Alligier
École Nationale de l'Aviation Civile
Université de Toulouse
Toulouse, France
richard.alligier@enac.fr

Hartmut Fricke
Chair for Air Transport Technology and Logistics
Technische Universität Dresden
Dresden, Germany
hartmut.fricke@tu-dresden.de

***Abstract*—With the aspiring development towards Trajectory-based Operations, novel tools for robust trajectory prediction are necessary. For this, the impact of uncertain input variables to the trajectory prediction must be understood to permit higher automation with increasing look-ahead times. In this study, a neural network provides input probability density functions for the aircraft mass and speed intent (multiple phases with constant calibrated air speed or Mach number). With our flight performance model, 10,000 climb phases are predicted in a Monte-Carlo simulation with a look-ahead time of 600 seconds for six different aircraft types. The resulting trajectory uncertainty is analyzed to prove that the stochastic characteristics of the input can be used to predict the arising uncertainties in future positions. Since the selected uncertainties are interdependent and time-lagged, the normality of the input vanishes in the trajectory uncertainty. However, a Beta distribution provides a good fit for up to 90% of the cases. The findings are applicable to decision support tools if the expected uncertainty shall be included.**

Keywords—Trajectory Uncertainty; Trajectory Prediction; Climb Phase; Neural Network; Monte-Carlo Simulation

I. INTRODUCTION

With the introduction of Trajectory-based Operations, all flights are represented by univocal, time-dependent trajectories. From the perspective of Air Traffic Management (ATM), a high level of predictability is required. Thus, the flights should adhere to their previously planned trajectories. From the operators' perspective, however, a certain level of flexibility is desired to react efficiently on uncertainties evolving during flight, e.g. due to imprecision in weather forecasts. Therefore, Trajectory Uncertainty must be included to provide a trade-off between these contrary interests. The Trajectory Uncertainty incorporates the likelihood for all deviations from the planned trajectory that may occur in the future. Thus, it is a stochastic extension to the well-known deterministic Trajectory Prediction (TP) process in ATM.

A deeper understanding of the uncertainty sources allows modeling of the resulting Trajectory Uncertainty. If the uncertainty source is represented by a probability density function (input PDF), the output PDF of the resulting Trajectory Uncertainty is likely to depend on this input PDF [1]. Therefore, it is beneficial for the TP when the input PDF of the uncertainty source is inferred from observations [2]. As a flight progresses, the Trajectory Uncertainty must be updated continuously as an integral part of the TP based on the observed behavior. Therefore, the following basic steps are applied:

1. Tracking of the flight (deterministic, e.g. current position);
2. Inference of unknown state variables (e.g. gross mass, speed intent) as stochastic input to the TP;
3. Prediction of the future aircraft track based on the derived state variables with re-assessment of the expected Trajectory Uncertainty; and finally
4. Decision support to Air Traffic Controllers based on conflict probabilities calculated from the Trajectory Uncertainty.

This study focuses on the *third* step, mainly on the prediction of future Trajectory Uncertainty with a given uncertainty in the state variables. Therefore, the COmpromised Aircraft performance model with Limited Accuracy (COALA) [3] is extended to predict trajectories of climbing aircraft with a Look-ahead Time (LAT) of 600 s. The predictions are based on real flight tracks provided by the OpenSky Network [4]. The gross mass and the speed intent during the climb (Calibrated Air Speed, CAS, and Mach number, altitude-dependent) are not included in the track data, so these values are inferred by a neural network as Gaussian input PDFs [2] to the TP. The procedure is called Cause-and-Effect Model and shown in Fig. 1.

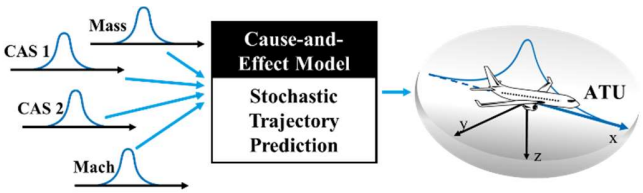

Fig. 1: Principle of the Cause-and-Effect Model, where probability density functions are provided for the uncertainty sources (left) to study the resulting Trajectory Uncertainty (right) after a given Look-ahead Time.

Due to the non-linear interaction of the uncertainty sources, a Monte-Carlo simulation is selected. The output of the Monte-Carlo simulation is analyzed with regard to three major areas: First, the correlation between the input PDFs and the resulting output PDFs is analyzed in order to understand the significance

Part of the project "Enhanced Flight Planning by introducing stochastic trajectory data", funded by Deutsche Forschungsgemeinschaft e.V.

978-1-7281-9825-5/20/$31.00 ©2020 IEEE

of each uncertainty source to the resulting Trajectory Uncertainty (Cause-and-Effect Model). Second, the outcome of the TP is compared to the tracks of the real flight. Finally, the increase in Trajectory Uncertainty over the LAT is analyzed to understand the robustness of a stochastic TP.

II. Theoretical Background

A. Trajectory Prediction

The capabilities for TP have been a key feature for ATM development for the past 25 years. The primary purpose of TP lies in predicting the future position of aircraft to provide assistance to the ATC controllers, e.g. for medium-term conflict detection or sequencing. In general, kinematic and kinetic TP are the two competing approaches [5]. Here, a kinetic TP is selected because it simulates the subjacent physical processes (in aviation: lift, drag, thrust force, and mass reduction due to fuel burn) and therefore allows to model uncertainties in the state variables that affect the physical aircraft behavior. For typical kinetic TP, the aircraft is simplified to a point mass model, commonly by using the required aircraft characteristics from the EUROCONTROL Base of Aircraft Data (BADA) [6]. Furthermore, a flight script must be provided to describe the flight intent (i.e. the sequence of planned maneuvers) to predict the speed and altitude profile [5]. Mondoloni et al. [7] provide various metrics to construe TP performance, analyzing input, output, outcome (output with a given input), and impact (false error vs. missed error rate). Typical Key Performance Areas include accuracy, confidence, stability, and reliability. In general, the prediction inaccuracy increases over time due to the accumulation of errors.

B. Trajectory Uncertainty

Besides uncertainties in the atmospheric forecasts, the flight intent and the state variables required for the kinetic TP are the main sources for prediction inaccuracies. The principle of Trajectory Uncertainty has been introduced to incorporate these inaccuracies in the TP. The Trajectory Uncertainty is divided into three Cartesian dimensions as the Along-Track Uncertainty (ATU), Vertical-Track Uncertainty (VTU), and Cross-Track Uncertainty (XTU) with reference to a certain point in time of the trajectory [1], [8]. Therefore, two different forms are used to characterize the Trajectory Uncertainty. On the one hand, the principle of Performance-Based Navigation [9] is applied by defining fixed bounds along the trajectory. Although these bounds are static values, they may be extended wherever higher uncertainties are expected, e.g. in the vicinity of the top of descent [10]. On the other hand, Trajectory Uncertainty is characterized stochastically, i.e. by representing each time step with a PDF [11]. The stochastic description requires additional data (e.g. type of PDF, shape parameters), but it also provides detailed insight into the likelihood of a particular position error. Furthermore, the stochastic description can be converted to fixed bounds easily by applying a bounding condition, e.g. $\pm 2\sigma$ for 95.45% of a Normal-distributed Trajectory Uncertainty, if required for a particular application.

For quantifying the Trajectory Uncertainty, various methods have been used. Rudnyk et al. [12] estimated prediction uncertainty for a LAT of 20 min with a Monte-Carlo simulation based on surveillance data sets (Automatic dependent surveillance-broadcast, ADS-B), where along-track errors of up to 18 NM and vertical-track errors up to 13,000 ft have been observed. Chatterji et al. [13] analyzed the impact of wind and temperature on the resulting Trajectory Uncertainty with Taylor Series expansions. Other model-based studies include Monte-Carlo simulation [14], [15], Polynomial Chaos Expansions [16], [17] and Bayesian Network theory [18].

C. Uncertainty Sources

Uncertainty Sources are the factors that induce the paramount part of the Trajectory Uncertainty. All state variables and other input to the TP are uncertainty sources if the exact value is not known. Typically, Uncertainty Sources are categorized as follows [19]:

- Forecast uncertainty: Uncertainties in the atmospheric modeling, especially wind speed and direction;
- Initial condition uncertainty: current state variables of the aircraft, e.g. gross mass;
- Intent uncertainty: control paradigm of the aircraft, e.g. intended cruise speed;
- Flight technical errors: inaccuracies in the flight control;
- Modeling errors, e.g. aircraft performance characteristics.

Understanding the stochastic characteristics of a certain Uncertainty Source and the resulting impact on the TP is the key to model the Trajectory Uncertainty from the source perspective. When analyzing the Trajectory Uncertainty of climbing aircraft, the calculation of the rate of climb ROC provides insight into the Uncertainty Sources in question. It contains the thrust force T, the drag force D, the TAS, the gross mass m, the gravitational acceleration g and the change in TAS depending on the altitude $dTAS/dh$ [6]:

$$ROC = \frac{dh}{dt} = \frac{(T-D)\cdot TAS}{m\cdot g}\left(1 + \frac{TAS}{g}\cdot\frac{dTAS}{dh}\right)^{-1} \quad (1)$$

First, the gross mass m is an Uncertainty Source that consists of the Actual Take-Off Mass uncertainty and fuel flow uncertainty (mass reduction during flight). The impact of the gross mass m has been analyzed as a part of FDR analysis [20], analytically [21], and in simulation studies [1], [14], which overall highlights its significance for climbing aircraft. Furthermore, the actual gross mass m remains an Uncertainty Source even if one would assume transmitting the mass via data link [22], since the actual take-off mass is never measured and therefore is only available as an estimate onboard.

Second, the "speed intent" is an Uncertainty Source. It is complex to model since it cannot be assumed that an aircraft climbs with a constant TAS. Instead, aircraft climb either with a constant CAS or constant Mach number M, depending on the current altitude and the local atmospheric conditions (temperature T and, for CAS only, air pressure p and atmospheric density ρ) [6]:

$$TAS_{\mathrm{CAS}} = \left[\frac{2}{\mu}\frac{p}{\rho}\left\{\left(1 + \frac{p_0}{p}\left[\left(1 + \frac{\mu}{2}\frac{\rho_0}{p_0}CAS^2\right)^{1/\mu} - 1\right]\right)^{\mu} - 1\right\}\right]^{0.5}$$

with:

$$\mu = (\kappa - 1)/\kappa \quad (2)$$

$$TAS_{\mathrm{Mach}} = M \cdot \sqrt{\kappa R T} \quad (3)$$

The equivalent TAS for constant CAS (red) and constant M (blue) depending on the altitude are shown in Fig. 2. For the graph, the atmospheric conditions have been simplified to the International Standard Atmosphere (ISA), which assumes a linear decrease in temperature below the tropopause and, thus, suggest an almost-linear dependency between Mach number and equivalent TAS:

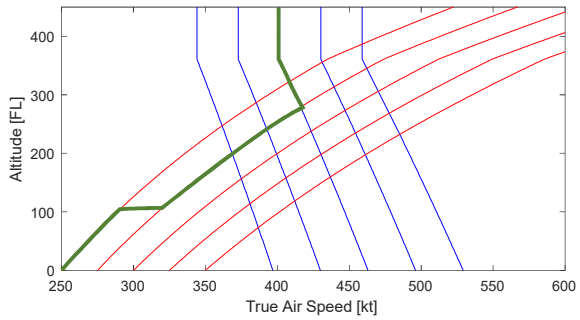

Fig. 2: Equivalent True Air Speed for constant Calibrated Air Speed (CAS) from 250 kt to 350 kt (red) and constant Mach number from 0.6 to 0.8 (blue) depending on the altitude under ISA conditions. The cross-over altitude is located where the blue and red line of the selected speed intent intersect. The green line indicates a typical speed profile for a climbing aircraft.

In consequence, the speed intent during the climb is segregated into two major phases: In the first phase with constant CAS, the aircraft accelerates continuously with respect to the equivalent TAS. In the second phase with constant M, the aircraft decelerates until it reaches the tropopause. The transition between acceleration and deceleration occurs at the cross-over altitude, where the selected CAS and M yield the same equivalent TAS. Thus, the cross-over altitude depends on the selected speed intent combination. These subjacent uncertainty sources result in an uncertainty in the cross-over altitude, which then increases the overall Trajectory Uncertainty due to the variety of observed speed intents.

Third, the thrust intent impacts the actual thrust force T and therewith the resulting rate of climb and the acceleration to the selected speed intent. Here, it is assumed that an aircraft uses its maximum climb thrust (MCMB) [6]; thus, no direct thrust intent uncertainty is considered. However, the resulting thrust is also influenced by the temperature, the air pressure, and the TAS.

Finally, the drag force D depends on the aircraft type, which is provided by BADA [6], and the TAS of the aircraft. Uncertainties in the drag polar itself are not considered here. Likewise, the gravitation acceleration g is constant, but the change due to the altitude is included in the geopotential altitude modeled by BADA. Intent Uncertainties other than the speed intent are excluded as well. It is assumed that a change in the lateral flight intent, whether it is desired by the flight crew, happens as a flight technical error or is instructed by the controller, will trigger a re-start of the TP.

D. *Inference of State Variables*

Since the discussed Uncertainty Sources, gross mass and speed intent, are not observed by the flight tracking, the actual value must be inferred. Reference [23] used an adaptive algorithm that adjusts a modeled mass in every successive TP based on the observed energy rate by reducing the difference to the modeled energy rate. This method was compared with a method, which estimates the mass by minimizing the quadratic error of the observed energy rate [24]. These analytical solutions reduce the TP error; however, do not provide an input PDF that could be used for a stochastic TP. Furthermore, most models estimate only one state variable because the number of unknown variables quickly increases when estimating multiple state variables, which requires more simplifying assumptions.

To overcome these disadvantages, various machine learning methods have been applied to the inference of state variables. A Kalman filter has been used to determine the TAS and the wind components based on the observed ground speed derived from radar data [25]. Various estimation methods for the initial mass have been combined by using Bayesian inference [26]. Reference [2] trained a neural network with ADS-B data of climbing aircraft, which then provides PDFs for the speed intent (CAS 1 below FL 100, CAS 2 until cross-over altitude and Mach number M) as well as for the equivalent mass m. In [27] the recursive Bayesian method called particle filtering is applied to estimate mass and thrust of climbing aircraft. Some machine learning methods, like the neural network, provide PDFs for the inferred state variables, which then are usable as input PDFs to a stochastic TP, as discussed in previous research [1]. Here, the work in [2] is used as input to our analysis.

III. Methodology

A. *Trajectory Prediction with Stochastic Input Variables*

To analyze the resulting Trajectory Uncertainty to form a Cause-and-Effect model, a Monte-Carlo simulation is performed with COALA. It calculates predictions of climbing aircraft with $LAT = 600$ s based on real flight data as well as inferred mass and speed intent PDFs provided by the neural network [2]. A non-disrupted climb is assumed, so the flight intent, other than the speed intent, is simplified to "continue climb". The simulation is conducted for six different aircraft types. For each aircraft type, the input data is segregated into segments of the same climb phase, which contain a varying number of prediction points with a temporal spacing of 15 s. For each of the prediction point, $N = 4{,}000$ different values for the mass and speed are sampled to calculate a prediction set. 10,000 prediction points per aircraft type, so 60,000 prediction points in total, each with 4,000 individual TPs are calculated. This data hierarchy is shown in Fig. 3:

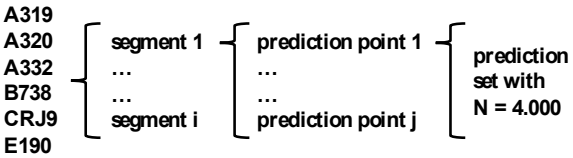

Fig. 3: Hierarchy of the data for the study, for each aircraft type multiple sets of segments i consist of j prediction points. A prediction set is calculated for each prediction point j with N = 4000 sampled aircraft states.

The simulation of each prediction set (see Fig. 4) uses the deterministic aircraft state variables and parameters of the Normal-distributed input PDFs from the neural network. With sampled values from the input PDFs, a climb phase is calculated with COALA, where altitude, TAS and still air distance are

logged every 15 s until LAT. These observations are collected for the entire prediction set for further analysis.

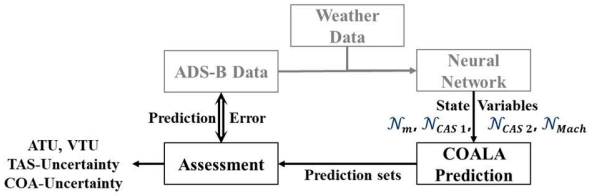

Fig. 4: Principle of the simulation for a single prediction set: The neural network components (grey, see [2]) provides state variables and input PDFs to simulate a set of stochastic trajectories (prediction set). Using the prediction set, the Trajectory Uncertainty is calculated and evaluated.

The assessment is done in stages starting with the analysis of all prediction sets of each aircraft type, for each segment, and finally for single prediction sets. Trial runs of several prediction sets have been conducted beforehand to determine the necessary number of predictions N per prediction point. For increasing N, the mean values of the observed TAS and altitude have been calculated. For $N \geq 3000$, the mean values remain almost constant (cf. Fig. 5). Thus, the number of predictions per segment is set to $N = 4000$.

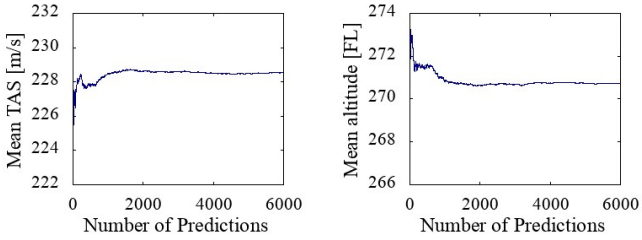

Fig. 5: Analysis of the observed mean True Air Speed and mean altitude depending on the number of predictions in the Monte-Carlo simulation, which converges to a constant value for more than 4000 runs.

B. Modeling of the Uncertainty Sources

The Uncertainty Sources modeled in this study are the mass and the speed intent using the output of a neural network. This neural network described in [2] models the conditional probability of the unknown state variables (m, $CAS\,1$, $CAS\,2$ and M) given the observed radar track of the considered flight. This information contains, for instance, the past points of the considered flight and forms the input of the neural network. Its output is the expected values μ and standard deviation σ of m, $CAS\,1$, $CAS\,2$, and M. These predicted μ and σ parameterize Normal distributions to model the uncertainty concerning these missing state variables. This neural network uses the trajectory data set described in [28]. It was trained on ten months of this data set and tested on two months. In this paper, using these two months of data, we compute the trajectory uncertainty using the mass and speed intent PDFs predicted by the neural network. These PDFs form the input of COALA.

The mass PDF describes the initial mass m at the beginning of the prediction point and is subject to mass reduction due to fuel burn. The speed intent is divided into $CAS\,1$ and $CAS\,2$ due to operational constraints, since the maximum speed is limited to 250 kt CAS below FL 100. Above the cross-over altitude, a third PDF for M describes the speed intent. As shown in Table 1, the initial state includes additional deterministic variables: the aircraft type, the current altitude, and TAS of the aircraft. Furthermore, a temperature profile is required for the speed conversion (cf. Equations (2) and (3)) and the flight performance calculation. This is derived from the Global Forecasting System (GFS) and has been extracted and prepared for the Neural Network. Since a Normal distribution is unbounded, values may be sampled that exceed the aircraft's limitations (below operating empty mass OEM, above maximum take-off mass MTOM, above maximum operating speed VMO or above maximum operating Mach number MMO). COALA is designed to reject such input to remain within the boundaries of the polynomial functions provided by BADA. Therefore, the sampling is checked in the analysis to ensure correct input PDFs. New random numbers are generated until $N = 4000$ acceptable samples are provided.

TABLE 1: INPUT DATA PROVIDED FOR EACH PREDICTION SET

Variable	Type	Source
Aircraft Type	deterministic	ADS-B [4]
Altitude	deterministic	ADS-B [4]
Current TAS	deterministic	ADS-B [4]
Temperature Profile	deterministic	GFS
Mass	$\mathcal{N}(\mu_m, \sigma_m)$	Neural Network [2]
Speed Intent $CAS\,1$	$\mathcal{N}(\mu_{\mathrm{CAS1}}, \sigma_{\mathrm{CAS1}})$	Neural Network [2]
Speed Intent $CAS\,2$	$\mathcal{N}(\mu_{\mathrm{CAS2}}, \sigma_{\mathrm{CAS2}})$	Neural Network [2]
Speed Intent Mach	$\mathcal{N}(\mu_{\mathrm{Mach}}, \sigma_{\mathrm{Mach}})$	Neural Network [2]

For a given speed intent, the actual speed observed at a given time depends on m, because it affects the climb rate, which then has a direct impact on the time until a change in the speed occurs. Furthermore, the combination of $CAS\,2$ and M changes the cross-over altitude, which adds another uncertainty to the time for the second speed intent change besides m. With that in mind, these uncertainty sources are interdependent and time-lagged (cf. Fig. 6). Therefore, it is not reasonable to assess one uncertainty after another (i.e. local sensitivity analysis). Instead, a global sensitivity analysis is performed.

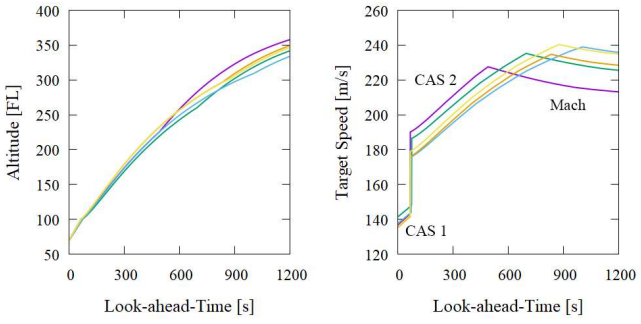

Fig. 6: Example of five trajectories with an A320 (left), where the speed intent transitions from CAS 1 to CAS 2 and Mach are clearly visible (right). The pink trajectory has a higher CAS 2 and a lower Mach number, which leads to a shallower climb in the CAS 2 phase that is compensated with a steeper climb after the lower cross-over altitude and Mach number compared to the set.

C. Flight Performance Model

The flight performance model COALA [3] has been developed for multi-criteria trajectory optimization with numerous target functions, where it has been used for air traffic

density assessment of freely optimized trajectories [29], flight planning [30] and inflight optimization [31], among others. It uses the BADA aircraft model files [6] (version 4 preferred, version 3 otherwise) for the calculation of drag, thrust, and fuel burn, but it facilitates a considerably extended approach using a proportional–integral–derivative (PID) controller to control acceleration and climb rate via the lift coefficient. For this study, COALA is extended to calculate trajectory segments for the TP with non-optimal target functions, e.g. constant CAS or M.

D. Analysis Methodology

Before the resulting trajectory uncertainty, the probabilities of exceeding the aircraft limitations are assessed with the input PDFs for $CAS\ 1$, $CAS\ 2$, M, and m at each prediction point. This is an indicator of deviations from the intended normal distribution due to the aircraft limitation considered by COALA. For the resulting trajectory uncertainty, we first assume normality and apply the Shapiro-Wilk test [32] with a significance level $\alpha = 0.05$ to the observations of the VTU (altitude at LAT), ATU (still air distance at LAT), TAS at LAT and the resulting cross-over altitude. Due to the non-linear dependencies, a total acceptance of the tests cannot be expected. Therefore, the analysis is then extended to Alpha, Beta, Chi and Gamma distributions. The Python library SciPy [33] is used to fit these PDF types with the Maximum Likelihood Estimate (MLE), while the best fit among the distributions is selected using the minimum Sum of Squared estimate of Errors (SSE). Furthermore, an assessment of all prediction points is conducted to understand the progression of the Trajectory Uncertainty over time. Here, some selected examples of significant prediction points are presented. Finally, the resulting Trajectory Uncertainty at LAT is compared to the actual altitude y of the radar tracks. To understand the applicability of the Trajectory Uncertainty and to compare the performance of an entire prediction set the relative altitude error $e_{\sigma,VTU}$ is calculated by normalizing the deviation of the radar track to the observed standard deviation σ_{VTU} of the VTU of each prediction point

$$e_{\sigma,VTU} = (y - \mu_{VTU}) \cdot {\sigma_{VTU}}^{-1} \tag{4}$$

IV. Results

A. Analysis of the Prediction Input

First, μ and σ of the input PDFs are used to compute the probabilities for speed intents and masses that exceed the aircraft type's limitations. For $CAS\ 1$, the probability of exceeding VMO is very low for all aircraft types and prediction points, as shown in Fig. 7. This is in line with the speed limit of 250 kt CAS below FL 100, which is well below VMO and correctly recognized by the neural network. In Fig. 8 a slight increase in the probability is visible for $CAS\ 2$, which still remains below 0.5% for most prediction points. Fig. 9 shows another increase in the probabilities for invalid values of M, where 5% to 40% of the prediction points exceed MMO with more than 0.5% probability. For m, cf. Fig. 10, the probabilities to exceed the MTOM are more than one order of magnitude higher compared to all speed intents. Especially for A332, CRJ9, and E190, the probability to exceed the MTOM is above 25% for up to one-third of the prediction points, reaching up to a 99% probability in some rare cases.

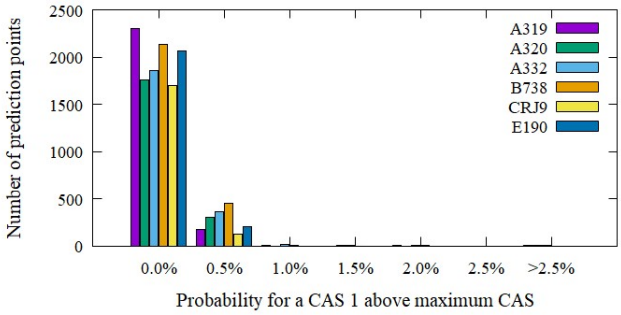

Fig. 7: Probabilities for the Calibrated Air Speed below FL 100 (CAS 1) to exceed the maximum CAS for each prediction point by aircraft type. It is very unlikely to exceed the CAS 1 because of the speed limit of 250 kt CAS below FL 100, which is correctly detected by the neural network.

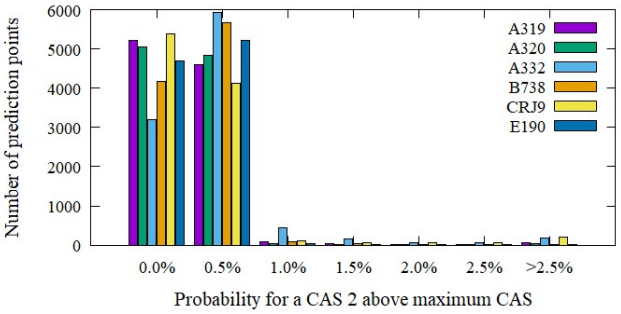

Fig. 8: Probabilities for a Calibrated Air Speed above FL 100 (CAS 2) to exceed the maximum CAS for each prediction point by aircraft type. The probabilities slightly increase in comparison to CAS 1 in Fig. 7, but still remain below 0.5%.

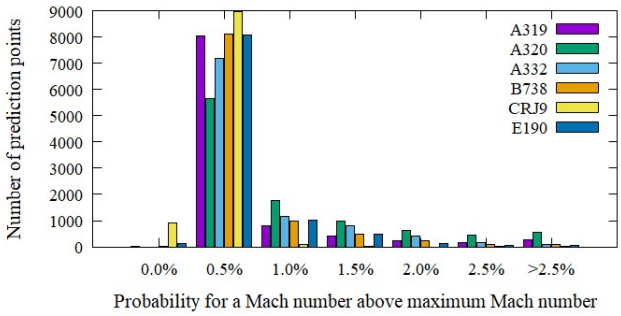

Fig. 9: Probabilities for a Mach number above the maximum Mach number for the aircraft type for each prediction point. Compared to the Calibrated Air Speed in Fig. 7 and Fig. 8, the probabilities are higher for the Mach number.

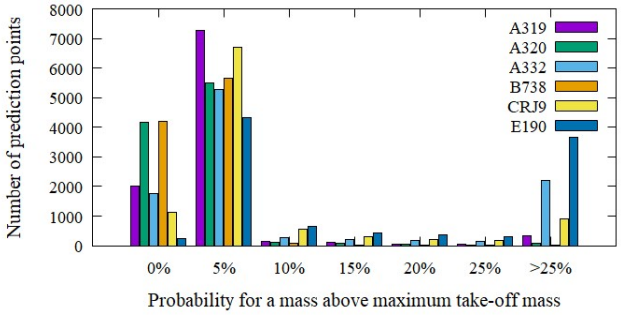

Fig. 10: Probabilities for a mass above the maximum take-off mass for each prediction point by aircraft type. Compared to the other uncertain inputs, the mass has a high probability for values outside the aircraft limitations, especially for the aircraft types A332, CRJ9, and E190.

Since COALA rejects any value above the limitation of the aircraft type, the normal distribution might be cut in the sampling for the Monte-Carlo simulation. Based on this analysis, the probability for cuts in the speed intents (CAS 1, CAS 2, and M) are very unlikely. For m, however, an impact of the cut input PDF must be expected.

B. Analysis of the Trajectory Uncertainty

To begin, the trajectory uncertainty is assumed to be normally distributed. In Table 2, the results of the Shapiro-Wilk tests on the output sampling are shown. The percentage differs from aircraft type to aircraft type. For instance, the A332 has the second-lowest count of accepted VTU samples, but a high number of accepted ATU samples. This is correlated to the higher probability of masses above MTOM (see Fig. 10), which affects the VTU stronger than the ATU. Despite the two to three changes in the speed intent, 6% to 22.5% of the flights show a Normal-distributed TAS at $LAT = 600$ s. Moreover, the cross-over altitude passes often, which is an indicator for the correlation between CAS 2 and M.

TABLE 2: RESULTS OF THE SHAPIRO-WILK TEST FOR THE OUTPUT PDFS' SAMPLING FOR 10,000 PREDICTION SETS PER AIRCRAFT TYPE

Aircraft Type	Percentage of Normal-distributed Observations			
	ATU	VTU	TAS	Cross-over
A319	8.0%	32.8%	14.5%	61.8%
A320	5.1%	31.4%	6.0%	48.8%
A332	31.3%	8.3%	14.3%	48.1%
B738	0.7%	39.8%	17.9%	57.9%
CRJ9	15.6%	13.0%	22.5%	50.4%
E190	12.2%	13.0%	20.0%	53.4%

The initial assumption of normally distributed output PDFs is then extended to a fitting for various other PDFs. Here, the Alpha, Beta, Chi, and Gamma distributions are selected based on the average shape of the output. Due to the high amount of data, the fitting is done automatically with SciPy [33] using MLE for the fitting itself and the minimum SSE for selecting the best fit among the distributions. For symmetrical samples, as shown in Fig. 11 for the ATU of a CRJ9, all selected PDFs provide a similar fit, with the Beta distribution being slightly better in this particular case.

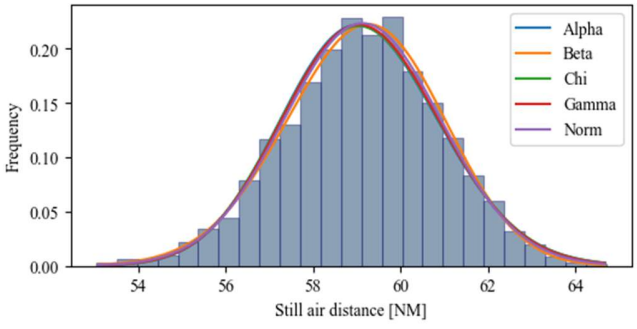

Fig. 11: Along-Track Uncertainty (ATU, still air distance in [NM]) for a CRJ9 at $LAT = 600$ s. In this case, the Beta distribution (orange, $\alpha = 83.9$ and $\beta = 38.7$) provides only a slightly better fit than the other functions.

As identified in the input PDF analysis, the A332 has a higher probability for masses above the MTOM. Especially for heavy aircraft like the A332, de-rated thrust is frequently used during climb when the aircraft load is low compared to the MTOM. With the initial assumption of MCMB, the neural network overestimates the real aircraft mass in consequence. This leads to a cut sampling of m due to the aircraft limitations considered by COALA. Since m has a significant impact on the climb rate, the VTU distribution is affected accordingly. Fig. 12 shows the VTU for one of these cases, where a Gamma distribution provides a significantly better fit due to the positive skew of the samples.

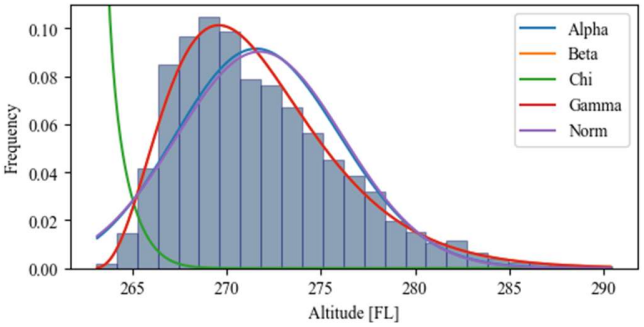

Fig. 12: Vertical-Track Uncertainty (VTU in [m]) of an A332 with high probabilities for masses above the aircraft limitation, where a significantly better fit is accomplished with the Gamma distribution (red, $\alpha = 4.1$) due to the positive skew of the samples.

The overall results for the fitting obviously differ depending on the type of Trajectory Uncertainty but also depending on the aircraft type. For the ATU, the vast majority of prediction sets yields similar results for all aircraft types. Approximately 90% of the ATU at $LAT = 600$ s can be fitted with a Beta distribution. Unlike the ATU, the VTU does not provide a clear result, because it has to account for both skewed and symmetric cases. Between 40% (B738) and 60% (A320) of the VTU fit best to the Beta distribution, while Alpha, Gamma, and Normal distribution yield similar fits of approximately 10% of the prediction points per aircraft type. Only the Chi distribution seldom fits in less than 3% of the cases. For the TAS at $LAT = 600$ s, the Beta distribution provides the best fit again for 58% to 76% of the prediction points for each aircraft type.

As expected and shown in Fig. 18, Trajectory Uncertainty increases with LAT. For convenience, this study focusses on $LAT = 600$ s.

C. Detail Analysis of Prediction Sets

1) Case 1: A319 with normally distributed trajectory uncertainty

This is a case of a prediction set with the aircraft type A319, where all Shapiro-Wilk tests on the output samples are accepted. As shown in Fig. 13 and Fig. 14, the ATU, VTU, cross-over altitude, and TAS are all Normal-distributed. In addition, with Fig. 15, the input mass is correlated with the output altitude. With Fig. 16, the air distance is correlated with CAS 2. These correlations are in line with the intuition; a high mass means the aircraft climbs slower, and a high speed intent means the aircraft flies faster. However, as we perform a global sensitivity analysis

(i.e. the other input variables are not constant), this shows that the randomness of the other input PDFs does not severely affect these expected correlations.

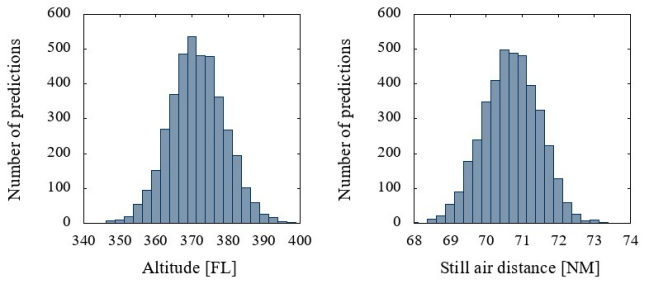

Fig. 13: Frequencies for Vertical-Track Uncertainty (VTU [FL], left), and Along-Track Uncertainty (ATU [NM], right) for an A319 after 600 s LAT that passed the Shapiro-Wilk test for normality.

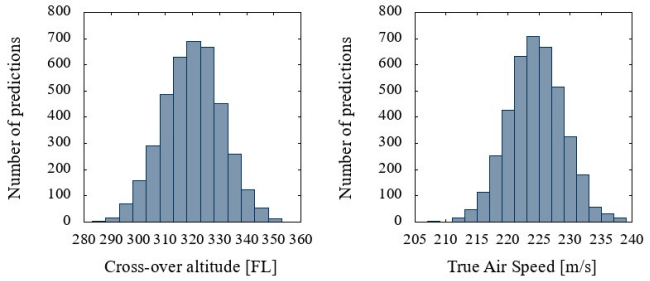

Fig. 14: Frequencies for the resulting cross-over altitude (left, [FL]), and the True Air Speed at LAT = 600 s (right, [m/s]) for an A319 that passed the Shapiro-Wilk test for normality.

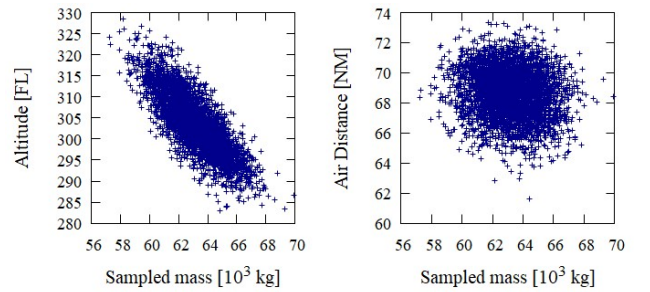

Fig. 15: Observed altitude (left) and still air distance (right) depending on the sampled mass for the A319 after 600 s LAT. A Correlation between altitude and mass is clearly visible, whereas the flown air distance does not depend on mass.

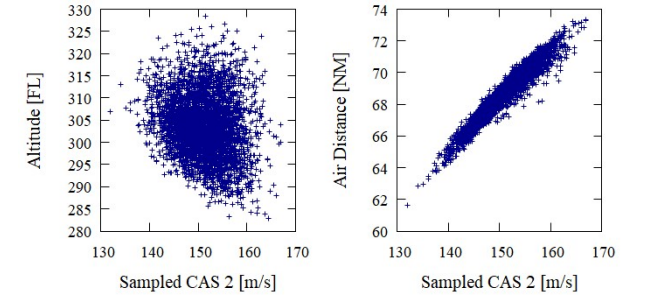

Fig. 16: Observed altitude (left) and still air distance (right) depending on the sampled speed intent CAS 2 for the A319 after 600 s LAT. As expected, a regression between air distance and speed can be detected, whereas altitude does not depend on speed.

2) *Case 2: A332 with a high probability above MTOM*

For the aircraft type A332, the analysis of the input PDFs showed a comparatively high probability of masses above the MTOM, which results in an asymmetrical sampling (left side of Fig. 17). The over-estimation in the mass is due to assuming MCMB, which is the highest thrust setting during the climb. Especially large aircraft, such as the A332, may use de-rated thrust instead.

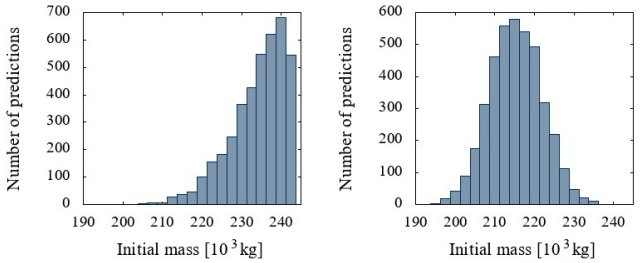

Fig. 17: Sampled masses from the input PDFs for the mass of the A332. On the left side, the input PDF has a high probability for masses above MTOM=242 tons, so those values are refused by COALA. Accordingly, the Shapiro-Wilk test fails; the samples are not Normal-distributed. The right side shows a passed test of another prediction point for comparison.

With the right tail missing in the mass distribution (left side in Fig. 17), one expects that the predicted trajectory uncertainty would over-estimate the rate of climb, leading to a steeper prediction compared to the actual radar track. In fact, the predicted VTU is shallower than the radar track, because the speed intent is over-estimated as well (cf. Fig. 18).

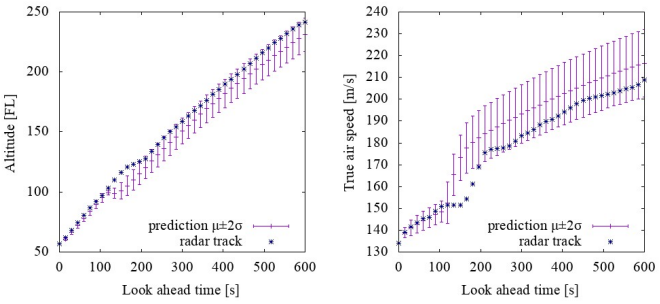

Fig. 18: Altitude profile (left) and change in TAS (right) of the predicted Trajectory Uncertainty (pink) compared to the actual radar track (blue) for the prediction point of the asymmetrically sampled mass of the A332 in Fig. 17.

3) *Case 3: B738 with two modes in ATU*

The aircraft type B738 has the lowest count of passed Shapiro-Wilk tests for the ATU of only 0.7% (cf. Table 2). Further analysis of prediction points where all other tests have been passed revealed that the ATU histogram contains a second mode, as shown in Fig. 19. Therefore, the hypothesis of a Normal-distributed ATU is rejected. $CAS\ 1$ is usually smaller than $CAS\ 2$ and the equivalent TAS of M is usually smaller than the TAS matching $CAS\ 2$. Thus, prediction points that fly a large part of the distance with $CAS\ 2$ will fly a greater overall distance than prediction points that fly mostly with $CAS\ 1$ or M. In this case, the Beta distribution provides a relatively better fit (orange line in Fig. 19).

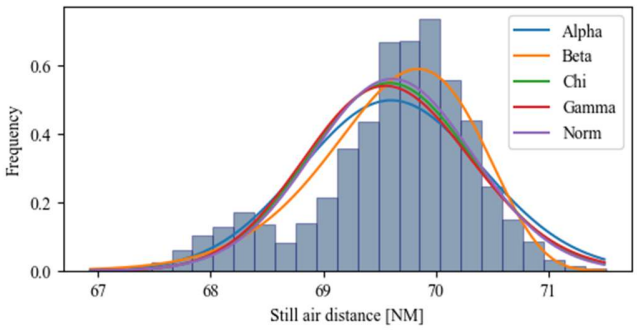

Fig. 19: Observed still air distance of the B738 at $LAT = 600$ s for a prediction point where the Shapiro-Wilk test failed, with fitting for other probability density functions. The best fit for this Along-Track Uncertainty is the Beta distribution (orange, with $\alpha = 695.97$ and $\beta = 9.25$).

D. *Comparison of the Trajectory Uncertainty with the Radar Tracks*

For comparing the radar tracks with the predicted uncertainty, the relative altitude error for all prediction points has been computed according to Equation (4). Fig. 20 shows the relative altitude error with respect to the observed standard deviation of the VTU for all aircraft types and all prediction points. The red line indicates the Required Navigation Performance (RNP) of 95% ≅ 2σ [8], [9]. With regard to the VTU, most actual trajectories remain inside the assumed RNP boundary of the Trajectory Uncertainty. However, some flights exceed the boundary with significantly high values of up to $10\sigma_{VTU}$.

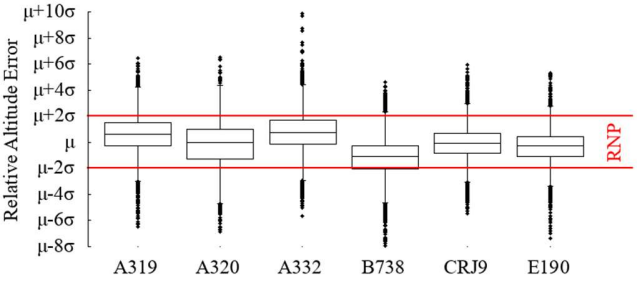

Fig. 20: Relative altitude error of the radar data at $LAT = 600$ s compared to the predicted Vertical Track Uncertainty relative to the observed standard deviation σ for all prediction sets of each aircraft type, with the RNP boundary of 95% ≅ 2σ in red.

V. Conclusion and Outlook

This study showed that, in principle, the input PDFs can be used to predict the resulting output PDF of the Trajectory Uncertainty. However, a simple approach using Normal distribution to model the output PDF cannot be used since almost 80% of the Trajectory Uncertainty is not Normal-distributed despite the moderate LAT of 600 s. Instead, a fitting with a Beta distribution is more suitable, since it accounts for possible skewness in the resulting Trajectory Uncertainty. Additionally, the assessment highlighted the sensitivity of the input PDFs. If the PDFs have a high probability for values outside the aircraft type's limitations and therewith outside of the polynomial functions provided by BADA, the resulting Trajectory Uncertainty is impaired as well. This is the case especially for the mass, which is based on the assumption of MCMB for the thrust.

Finally, we have to note that wind uncertainty was not considered in this study. However, all predictions refer to the aerodynamic coordination system, see Equation (1). Therefore, altitude and TAS profiles calculate here can be applied to the wind information. Furthermore, COALA is able to run the TP with GRIB2 weather data, if provided.

Acknowledgment

The authors like to thank Stanley Förster for maintaining COALA continuously and for providing valuable insight into all software-related challenges along with our work.

References

[1] T. Zeh, J. Rosenow, and H. Fricke, "Interdependent Uncertainty Handling in Trajectory Prediction," Aerospace, vol. 6, no. 2, p. 15, Feb. 2019.

[2] R. Alligier, "Predictive Distribution of the Mass and Speed Profile to Improve Aircraft Climb Prediction," presented at the 13th USA/Europe Air Traffic Management Research and Development Seminar (ATM2019), Vienna, Jun. 2019.

[3] J. Rosenow and H. Fricke, "Flight performance modeling to optimize trajectories," presented at the Deutscher Luft- und Raumfahrtkongress (DLRK), 2016.

[4] "The OpenSky Network - Free ADS-B and Mode S data for Research." https://opensky-network.org/datasets/publication-data/climbing-aircraft-dataset/ (accessed Nov. 11, 2019).

[5] S. Swierstra and S. Green, "Common Trajectory Prediction Capability for Decision Support Tools," presented at the 5th USA/EUROPE Air Traffic Management R&D Seminar, Budapest, 2003.

[6] "User Manual for the Base of Aircraft Data (BADA) Family 4," European Organisation for the Safety of Air Navigation (EUROCONTROL), EEC Technical/Scientific Report No. 12/11/22-58, Mar. 2016.

[7] S. Mondoloni, S. Swierstra, and M. Paglione, "Assessing Trajectory Prediction Performance - Metrics Definition," in 24th Digital Avionics Systems Conference, Washington, DC, USA, 2005, vol. 1, p. 3.C.1-1-3.C.1-13.

[8] T. Pabst, T. Kunze, M. Schultz, and H. Fricke, "Modeling external disturbances for aircraft in flight to build reliable 4D trajectories," presented at the 3rd International Conference on Application and Theory of Automation in Command and Control Systems, Jan. 2013.

[9] International Civil Aviation Organization, Ed., Performance-based navigation (PBN) manual, 3rd ed. Montréal: ICAO, 2008.

[10] R. A. Paielli, "Trajectory Specification Language for Air Traffic Control," J. Adv. Transp., vol. 2018, pp. 1–10, 2018.

[11] H. Jeung, H. Lu, S. Sathe, and M. L. Yiu, "Managing Evolving Uncertainty in Trajectory Databases," IEEE Trans. Knowl. Data Eng., vol. 26, no. 7, pp. 1692–1705, Jul. 2014.

[12] J. Rudnyk, J. Ellerbroek, and J. M. Hoekstra, "Trajectory Prediction Sensitivity Analysis Using Monte Carlo Simulations Based on Inputs' Distributions," J. Air Transp., pp. 1–18, Aug. 2019.

[13] G. Chatterji, Gano Broto, B. Sridhar, and K. Bilimoria, "En-route flight trajectory prediction for conflict avoidance and traffic management," presented at the Guidance, Navigation, and Control Conference, San Diego,CA,U.S.A., Jul. 1996, Accessed: Apr. 16, 2020. [Online]. Available: http://arc.aiaa.org/doi/10.2514/6.1996-3766.

[14] J. Kim, M. Tandale, and P. K. Menon, "Air-Traffic Uncertainty Models for Queuing Analysis," presented at the 9th AIAA Aviation Technology, Integration, and Operations Conference (ATIO), Hilton Head, SC, Sep. 2009.

[15] M. Schultz et al., "Modelling and Evaluation of Automated Arrival Management Considering Air Traffic Demands," presented at the 3rd SESAR Innovation Days, 2013.

[16] X. Li, P. B. Nair, Z. Zhang, L. Gao, and C. Gao, "Aircraft Robust Trajectory Optimization Using Nonintrusive Polynomial Chaos," J. Aircr., vol. 51, no. 5, pp. 1592–1603, Sep. 2014.

[17] E. Casado, M. L. Civita, M. Vilaplana, and E. W. McGookin, "Quantification of aircraft trajectory prediction uncertainty using polynomial chaos expansions," presented at the 2017 IEEE/AIAA 36th Digital Avionics Systems Conference (DASC), St. Petersburg, FL, Sep. 2017.

[18] Á. Rodríguez-Sanz, F. Gómez Comendador, R. M. Arnaldo Valdés, J. A. Pérez-Castán, P. González García, and M. N. G. Najar Godoy, "4D-trajectory time windows: definition and uncertainty management," Aircr. Eng. Aerosp. Technol., p. AEAT-01-2018-0031, Dec. 2018.

[19] E. Casado, C. Goodchild, and M. Vilaplana, "Identification and Initial Characterization of Sources of Uncertainty Affecting the Performance of Future Trajectory Management Automation Systems," presented at the ATACCS'2012, London, May 2012.

[20] M. Uzun and E. Koyuncu, "Data-Driven Trajectory Uncertainty Quantification For Climbing Aircraft To Improve Ground-Based Trajectory Prediction," ANADOLU Univ. J. Sci. Technol. - Appl. Sci. Eng., pp. 323–345, Jun. 2017.

[21] R. Vazquez and D. Rivas, "Propagation of Initial Mass Uncertainty in Aircraft Cruise Flight," J. Guid. Control Dyn., vol. 36, no. 2, pp. 415–429, Mar. 2013.

[22] R. A. Coppenbarger, G. Kanning, M. Field, and R. Salcido, "Real-Time Data Link of Aircraft Parameters to the Center-TRACON Automation System (CTAS)," presented at the 4th USA/EUROPE Air Traffic Management R&D Seminar, Santa Fe, NM, Dec. 2001.

[23] D. Thipphavong, C. Schultz, A. Lee, and S. Chan, "Adaptive Algorithm to Improve Trajectory Prediction Accuracy of Climbing Aircraft," J. Guid. Control Dyn., vol. 36, no. 1, pp. 15–24, Jan. 2013.

[24] R. Alligier, D. Gianazza, M. Ghasemi Hamed, and N. Durand, "Comparison of Two Ground-based Mass Estimation Methods on Real Data," presented at the 6th International Conference on Research in Air Transportation (ICRAT 2014), Istanbul, May 2014.

[25] D. Delahaye and S. Puechmorel, "TAS and wind estimation from radar data," in IEEE/AIAA 28th Digital Avionics Systems Conference, Orlando, FL, USA, Oct. 2009, p. 2.B.5-1-2.B.5-16.

[26] J. Sun, J. Ellerbroek, and J. M. Hoekstra, "Bayesian Inference of Aircraft Initial Mass," presented at the 12th USA/Europe Air Traffic Management Research and Development Seminar (ATM2017), Seattle, WA, 2017.

[27] J. Sun, H. A. P. Blom, J. Ellerbroek, and J. M. Hoekstra, "Aircraft Mass and Thrust Estimation Using Recursive Bayesian Method," presented at the 8th International Conference on Research in Air Transportation (ICRAT2018), Castelldefels, 2018.

[28] R. Alligier and D. Gianazza, "Learning aircraft operational factors to improve aircraft climb prediction: A large scale multi-airport study," Transp. Res. Part C Emerg. Technol., vol. 96, pp. 72–95, Nov. 2018.

[29] J. Rosenow, S. Förster, M. Lindner, and H. Fricke, "Impact of Multi-critica Optimized Trajectories on European Air Traffic Density, Efficiency and the Environment," presented at the 12th USA/Europe Air Traffic Management Research and Development Seminar (ATM2017), Seattle, WA, 2017.

[30] M. Lindner, J. Rosenow, S. Förster, and H. Fricke, "Potential of integrated flight scheduling and rotation planning considering aerodynamic-, engine- and mass-related aircraft deterioration," CEAS Aeronaut. J., Nov. 2018.

[31] M. Lindner, J. Rosenow, T. Zeh, and H. Fricke, "In-flight aircraft trajectory optimization within corridors defined by ensemble weather forecasts," presented at the International Conference for Research in Air Transportation (ICRAT 2020), Tampa, FL, 2020.

[32] S. S. Shapiro and M. B. Wilk, "An Analysis of Variance Test for Normality (Complete Samples)," Biometrika, vol. 52 (3–4), pp. 591–611, 1965.

[33] P. Virtanen et al., "SciPy 1.0: fundamental algorithms for scientific computing in Python," Nat. Methods, vol. 17, no. 3, Art. no. 3, Mar. 2020.